Mon. Not. R. Astron. Soc. **000**, 1–?? (2011) Printed 5 June 2012 (MN LaTeX style file v2.2)

Spectral and temporal analysis of the joint *Swift*/BAT-*Fermi*/GBM GRB sample

Francisco J. Virgili[1,2⋆], Ying Qin[3], Bing Zhang[2], and Enwei Liang[3]
[1] *Astrophysics Research Institute, Liverpool John Moores University, Birkenhead CH41 1LD, UK*
[2] *Department of Physics and Astronomy, University of Nevada Las Vegas, Las Vegas, NV 89154, USA*
[3] *Department of Physics and Astronomy, Guangxi University, Nanning 530004, China*

Accepted xxxx. Received xxxxx; in original form xxxxx

ABSTRACT

Using the gamma-ray bursts simultaneously detected by *Swift*/BAT and *Fermi*/GBM we performed a joint spectral and temporal analysis of the prompt emission data and confirm the rough correlation between the BAT-band photon index $\Gamma^{\rm BAT}$ and the peak spectral energy $E_{\rm peak}$. With the redshift known sub-sample, we derived the isotropic gamma-ray energy $E_{\gamma,\rm iso}$ and also confirm the $E_{\gamma,\rm iso} - E_{\rm peak,rest}$ relation, with a larger scatter than the Amati sample but consistent with GBM team analyses. We also compare the T_{90} values derived in the GBM band with those derived in the BAT band and find that for long GRBs the BAT T_{90} is usually longer than the GBM T_{90}, while for short GRBs the trend reverses. This is consistent with the soft/hard nature of long/short GRBs and suggests the importance of an energy-dependent temporal analysis of GRBs.

Key words: gamma-rays: bursts

1 INTRODUCTION

Since the launch of the *Fermi* satellite in 2008, a significant number of gamma-ray bursts (GRBs) have been observed by both the *Fermi* Gamma-ray Burst Monitor (GBM, 8 keV-40 MeV) and *Swift* (Gehrels et al. 2004). Since the energy band of *Swift* BAT is narrow (15-150 keV) and the peak of the spectrum is often outside the observed energy window (Sakamoto et al. 2009), the joint BAT-GBM sample is valuable for *Swift* science by providing important information about the prompt emission, especially the characteristic peak energy of the νF_ν spectrum, $E_{\rm peak}$. Using the *Fermi*/GBM-*Swift*/BAT joint sample we performed a two-part analysis on the prompt emission data. First, a joint spectral analysis where we fit the data from both detectors and investigated several empirical correlations. Second, a temporal analysis where we rigorously derived T_{90} in the 8-1000 keV band and compared it to the published BAT values.

A variety of empirical relations have been discussed in the literature (Amati et al. 2002; Amati 2003; Sakamoto et al. 2004; Sakamoto et al. 2006; Ghirlanda et al. 2004; Liang & Zhang 2005; Yonetoku et al. 2004), many of which utilize $E_{\rm peak}$. Since $E_{\rm peak}$ cannot be well measured for most *Swift* GRBs, efforts have previously been made to look for indicators of $E_{\rm peak}$ based on the available observed quantities. In particular, the effective photon power law index in the BAT band, $\Gamma^{\rm BAT}$, has been found to be broadly correlated with $E_{\rm peak}$. Two versions of this relation are found in the literature: one presented in Sakamoto et al. (2009) using simulations of BAT spectra and $E_{\rm peak}$ measurements from broad-band detectors (e.g. Konus-Wind), and another presented in Zhang et al. (2007b) with $E_{\rm peak}$ estimates based on the hardness ratio in the BAT band itself (Zhang et al. 2007a; see also Cui et al. 2005). In §3.2 we re-calibrate this correlation with the GBM-BAT joint sample. The $E_{\gamma,\rm iso} - E_{\rm peak,rest}$ relation (or Amati relation; Amati et al. 2002; Amati 2003) is one of the most widely studied, and hotly debated, empirical correlations that may connect to GRB physics (e.g. Band & Preece 2005; Nakar & Piran 2005; Kocevski 2011). In §3.3 we test the Amati relation with the redshift-known sub-sample of the GBM-BAT joint sample.

Finally, traditionally long and short GRBs were defined in the BATSE band with a separation of about 2 seconds in the observed frame (Kouveliotou et al. 1993). When applied to *Swift* GRBs and combined with multi-wavelength afterglow data, this definition creates confusion when used for GRB classification (e.g. Zhang et al. 2007b, 2009). Since the energy band of GBM is similar to that of BATSE, a comparison between the measured T_{90} durations in the two detectors is of great interest and is performed in §4.

⋆ E-mail: fjv@astro.livjm.ac.uk (FJV)

2 SAMPLE AND DATA REDUCTION

We conducted our analysis on the sample of GRBs that were observed simultaneously with the *Swift*/BAT and *Fermi*/GBM detectors. The sample was chosen from bursts that were consistent both temporally (similar trigger times in *Swift* MET) and in sky placement (RA/DEC) between June 2008 and May 2011. Our final sample consists of 75 bursts whose spectra were fit individually to check consistency with the literature and then fit jointly. Some bursts were removed because they were a *Swift* ground detection (e.g. 100427A; partial data) or a false detection (e.g. 080822B which has been classified as an SGR flare).

The *Fermi*-GBM GRB data was downloaded from the online *Fermi* GRB burst catalog found on the NASA HEASARC website[1] and the time-integrated spectra were fit with the GBM software `RMfit`[2]. The *Swift*-BAT data was downloaded from the *Swift* data table, also located on the NASA HEASARC website[3]. The resulting data was processed using the typical *Swift*-BAT products (`batgrbproduct`) after updating to the current calibration database (`bateconvert`) to create the burst lightcurves and spectra.

3 SPECTRAL ANALYSIS

3.1 Results

We performed spectral fits for the GBM GRBs with `RMfit` using the built-in power law (PL), power law with exponential cutoff (CPL, 100 keV normalization energy) and Band function (Band et al. 1993) models over the entire burst temporal and spectral (8 keV-40 MeV) interval in order to determine the best fit model. The goodness of the fits are measured with the C-statistic. If the C-stat was comparable for two models, the simpler model (i.e. the one with less parameters) was chosen as the better fit to compensate for the added degree of freedom. On many occasions, the decrease in the statistic was greater than 30-50 for a PL versus a CPL fit, for example, but not significantly reduced when comparing the CPL and Band function fit. Evidence of this can be seen in the majority of CPL fits in the GBM data summarized in Tables 1 and 2. The spectral regime chosen for the NaI detectors was roughly 8-900 keV and 200 keV-40 MeV for the BGO detectors. Our spectral fit results are generally consistent with the literature (e.g. Bissaldi et al. 2011; Nava et al. 2011; individual burst GCN reports).

For BAT spectral fitting, it is important to make sure that the the satellite was not slewing during data acquisition. If *Swift* was slewing while capturing a spectrum, a new weighted response file was created to compensate for the motion (Sakamoto et al. 2011). The response matrices are created in 5 second intervals and weighted to created a final response file that is used with the total spectrum. Each time-integrated spectrum was fit over the full BAT energy range of 15-150 keV using the same three models listed above. If a model showed improvement greater than $\Delta\chi^2 > 6$ per added degree of freedom then that model was deemed a better fit. Our spectral fitting for the BAT data and joint spectral fits for the GBM and BAT observed spectra are performed with Xspec. We re-bin the spectra with the criterion that the number of photon counts per bin is greater than 20 by using the HEAsoft tool *grppha* if the burst was sufficiently short or weak that this procedure was warranted. In order to address the calibration between the BAT and the GBM NaI/BGO detectors, each spectrum was fit with a varying calibration constant. The BAT calibration was fixed to 1.0 and the NaI and BGO constants were left as free parameters to be fit. About half of the bursts did not produce reliable fits to the BGO detector calibration constant, likely due to the sometimes low signal in the BGO detector. For these bursts the BGO constant was fixed to the mean value of the distribution of BGO calibration constants (1.3) and the spectra were refit. The χ^2 and spectral parameter errors were generally reduced when compared to the fits where all the calibration constants were forced to be equal.

The best-fit spectral models of all the 75 bursts in the joint GBM-BAT sample are presented in Table 1 (simple powerlaw model) and Table 2 (cutoff powerlaw or Band models). The distributions of $E_{\rm peak}$ and α of the sample are shown in Fig. 1. The results are generally consistent with previous results (e.g. Preece et al. 2000; Zhang et al. 2011; Nava et al. 2011). The $E_{\rm peak}$ distribution is roughly log-normal but is somewhat wider than that of the bright BATSE GRB sample (Preece et al. 2000). Our sample includes GRBs in a broader $E_{\rm iso}$ range, broadening the observed $E_{\rm peak}$ range. The low-energy spectral index α peaks around 1 as suggested by previous works. We do not present the distribution of the high energy photon index β due to the small sample size (most spectra can be fit by a cutoff powerlaw model). Although they form a limited part of our sample the distribution for short bursts show behavior consistent with previous samples, namely a harder median $E_{\rm peak}$ and similar or slightly shallower pre-break slope.

Since the GBM energy band covers that of BAT, we also derive $E_{\rm peak}$ with the GBM data only and compare the values with the joint fit values. Figure 2 shows the relationship between the separately derived GBM and joint sample $E_{\rm peak}$ values with a line of slope 1 drawn for reference, showing the generally small differences between the samples.

3.2 $\Gamma^{\rm BAT} - E_{\rm p}$ relation

With our spectral analysis results, we examine the empirical relations between the PL slope of the BAT spectrum, $\Gamma^{\rm BAT}$, and $E_{\rm peak}$ proposed by Sakamoto et al. (2009) and Zhang et al. (2007b):

$$\log E_{\rm peak} = 3.258 - 0.829\Gamma^{\rm BAT} \quad (1)$$

and

$$\log E_{\rm peak} = (2.76 \pm 0.07) - (3.61 \pm 0.26) \log \Gamma^{\rm BAT}, \quad (2)$$

respectively[4]. Both Zhang et al. (2007a,b) and Sakamoto et al. (2009) indicate that the relation is valid between slopes

[1] http://heasarc.gsfc.nasa.gov/W3Browse/fermi/fermigbrst.html
[2] fermi.gsfc.nasa.gov/ssc/data/analysis/
[3] http://heasarc.gsfc.nasa.gov/cgi-bin/W3Browse/swift.pl

[4] Sakamoto et al. (2009) derive 1σ error levels which are based on the value of Γ (see their Table 1): Lower limit: $-20.684 + 43.646\Gamma - 26.891\Gamma^2 + 5.185\Gamma^3$ Upper limit: $-5.198 + 16.568\Gamma - 10.630\Gamma^2 + 2.034\Gamma^3$

of roughly $1.2 < \Gamma^{\rm BAT} < 2.3$. Here we aim to present the entire data set of the joint sample and see how the relation fares over the entire observable sample. It is also interesting to explore whether using the joint spectra is consistent with the derivation of $E_{\rm peak}$ from using only the GBM sample and a motivation for investigating the combined constraints of the two detectors.

Using only the 53 joint sample bursts that had BAT spectra best fit with a PL function and the joint spectra $E_{\rm peak}$, regardless of whether it is from a CPL or Band function, we derive relations that are steeper than the values above (Figure 3). The ordinary least squares method gives shallower slopes more consistent with the values of Sakamoto (2009) and the bisector fits are steeper and more consistent with the values presented in Zhang et al. (2007b). Below we summarize the bisector fits, assuming these produce more reliable fits that take into account the intrinsic scatter of the distribution:

$$\log E_{\rm peak} = (4.40 \pm 0.509) - (1.31 \pm 0.148)\Gamma^{\rm BAT} \quad (3)$$

$$\log E_{\rm peak} = (3.05 \pm 0.359) - (3.79 \pm 0.554) \log \Gamma^{\rm BAT} \quad (4)$$

Using the values of $E_{\rm peak}$ from either a CPL or Band function fit is a valid assumption, as shown in Figure 4. This figure shows the values of $E_{\rm peak}$ derived from both models together with the best-fit line, which has a slope very close to 1.

Next we look at all the bursts in the sample, including those whose BAT spectra are fit with a CPL model. Since the relations above deal with the PL slope of the BAT spectrum, we forced the remaining CPL bursts to be fit with a PL model to see if the relationships changed in any way (Fig 5). The results are similar, with the slopes becoming slightly steeper than the previous values:

$$\log E_{\rm peak} = (4.34 \pm 0.475) - (1.32 \pm 0.129)\Gamma^{\rm BAT} \quad (5)$$

$$\log E_{\rm peak} = (3.00 \pm 0.332) - (3.88 \pm 0.469) \log \Gamma^{\rm BAT} \quad (6)$$

Lastly, Figure 6 shows the relationship between $\Gamma^{\rm BAT}$ and the joint CPL/Band fit spectral slope α. The data all lie below the reference line of $\alpha = \Gamma^{\rm BAT}$. This is understandable, since the effective photon index $\Gamma^{\rm BAT}$ has to compensate for the curved spectrum around $E_{\rm peak}$ and is, therefore, generally steeper. The scatter in the relative steepness is related to the location of $E_{\rm peak}$. The larger the $E_{\rm peak}$, the closer $\Gamma^{\rm BAT}$ to α. If $E_{\rm peak}$ is relatively low, the BAT-band spectra are severely bent and the effective $\Gamma_{\rm BAT}$ could be very different from α.

3.3 Amati Relation

A sub-sample of 25 GRBs in GBM-BAT joint sample have measured redshifts. With this value we can calculate the isotropic energy released which, combined with the rest-frame peak spectral energy, $E_{\rm peak,rest}$, can be used to test the empirical Amati relation (Amati et al. 2002; Amati 2003). Since our spectral fits are derived from time-integrated spectra, we can derive the mean energy flux F during the extracted time scale Δt (which is essentially T_{90}) in a desired energy band, which we uniformly adopt as the rest-frame 1-10^4 keV energy flux. We worked on only bursts whose time integrated spectra are fit by a Band function of CPL, therefore three bursts that are fit with a simple PL in the z-known sub-sample are excluded. We then derived the broad-band isotropic γ-ray energy $E_{\rm iso} = 4\pi d_L^2 F \Delta t/(1+z)$, where Δt is the time interval over which the spectral fit was derived, d_L is the luminosity distance, and the factor of $(1+z)$ is the correction for cosmological time dilation. If the spectrum is best described by a CPL then the best-fit pre-break slope (α) is used with the assumption of a typical β of -2.3 to construct a Band function. Otherwise, the best-fit Band function parameters are used. In Figure 7 we present the differences between deriving the flux from a CPL as opposed to a Band function. The calculated fluence (and therefore $\rm E_{iso}$) is systematically underestimated by a mean factor of 1.4 and a maximum of 2 for this sample. For the bursts that are best fit with a CPL we also refit the spectra with a Band function and use those spectral parameters, even though this model has a larger χ^2, to derive $E_{\rm iso}$. These results are also included in Figure 7 and show that the bursts tend to follow a similar, although not identical, distribution as the CPL fits.

We fit the Amati relation sample with two different methods: ordinary least squares and ordinary least squares bisector fit, the latter an accepted method to fit linear models while taking into account some of the scatter of the data set. We provide both fits for comparison, although the bisector method is likely a more accurate depiction of the true relation. For the joint sample these methods give differing solutions that we explore below. First, using the ordinary least squares method, our results are generally consistent with slopes for the $E_{\rm peak,rest} - E_{\rm iso}$ relation presented in the literature (Amati et al. 2008; Zhang et al. 2009; Ghirlanda et al. 2009; Ghirlanda et al. 2010; Amati 2010; Gruber et al. 2011), having a slope of 0.5 but a larger normalization (see Figure 8). Using the bisector fit we find that the slope steepens significantly to 0.76, with a lower intercept. This steepening, however, is due to a selection effect in the data owing to a lack of bursts above an energy of about 10^{54} erg. The highest energy bursts reported by *Fermi* (e.g. 080916C, 090323) are not simultaneously detected by *Swift* and are not included in our sample. Adding in the three highest energy *Fermi* bursts by hand to simulate a more unbiased sample (data from D. Gruber, private communication), the relation drops down to 0.57, which is fully consistent with previous estimates and serves as a consistency check for our sample. In general, we derive a larger scatter in the Amati relation than the sample presented in works such as Amati et al. (2008, 2010). The results are consistent, however, with another independent analysis of the GBM bursts (Gruber et al. 2011). The mean and median of the $E_{\rm iso}$ distribution of our sample are 8.4×10^{52} erg and 6.07×10^{52} erg, respectively. Figure 8 shows the $E_{\rm peak,rest} - E_{\rm iso}$ relationship for the 20 bursts of the joint sample with known redshift with the linear bisector fit as well as an approximation of the fits by Gruber et al. (2011; blue/solid) and Amati et al. (2008; red/dashed) with their respective 2σ regions. The outlier of the distribution, having an $E_{\rm peak,rest}$ of about 8000 keV, is GRB 090510. It is the only redshift-known short burst in the sample. Previous works have shown that short ($T_{90} < 2$ sec) bursts follow a different relationship and are not included in the slope determination of the longer bursts (Amati et al. 2008; Zhang et al. 2009; Ghirlanda et al. 2009; Amati 2010).

4 COMPARISON OF BURST DURATIONS IN THE BAT AND GBM BANDS

We calculate the T_{90} values observed in the GBM band for the bursts in our sample by using a Bayesian Block method (Scargle 1998; Richardson et al. 1996). The lightcurves we use are in 64 ms bins and are extracted from the brightest NaI detector. With the Bayesian Block method we derive T_5 and T_{95}, the epochs when 5% and 95% of the total fluence were registered, respectively. We then derive T_{90} by $T_{90} = T_{95} - T_5$ with the errors of T_5 and T_{95} estimated with the bootstrap method and assuming that the observed errors in the lightcurves are log-normal. We generate 1000 mimic lightcurves from the error distributions and calculate their T_{90} for a given burst. We make a Gaussian fit to the T_{90} distributions then derive the value of T_{90} and its 1σ error. T_{90} in the BAT band is taken from the Second BAT Catalog (Sakamoto et al. 2011) (bursts before 2010) and GCN reports (bursts after 2010; see Table 3 for specific references).

A comparison of the T_{90} in the BAT and GBM bands along with their distributions is shown in Figure 9. It is found that the distributions are still bimodal. The T_{90} measured in the BAT band for long GRBs is usually larger than that in the GBM band. However, the T_{90} measured in the BAT band for short GRBs is even shorter than that in the GBM band. Since BAT is more sensitive to softer emission than GBM, this fact is consistent with the soft/hard nature of long/short GRBs, respectively. In particular, fainter, softer emission can be picked up by BAT but not by GBM, so that T_{90}(BAT) can be much longer than T_{90}(GBM) in some bursts. Conversely, since short GRBs are typically hard, BAT may not be sensitive enough to pick up some emission episodes that GBM can. As a result, T_{90} of short GRBs can be longer in the GBM band than in the BAT band.

The difference in T_{90} for different detectors may also affect the derivation of the isotropic energy. This is because some long bursts having shorter T_{90} in the GBM band than BAT band may be sampling only the hardest and brightest part of the spectrum. For the small sample of six bursts above the Amati et al. 2σ region in Fig. 8 we find that all have longer durations in the BAT bands with half of them significantly longer (difference $> 30\%$), which may indicate the existence of this spectrum sampling effect. This suggests that in order to fully characterize the durations, and hence, the physical origin of the bursts, multi-band data and a careful energy-dependent temporal analysis are essential (see Qin et al. 2012).

5 CONCLUSIONS AND DISCUSSION

Using the data available from *Fermi* and *Swift* we performed an analysis of the jointly detected GRB sample. The spectral analysis indicates that fitting the joint spectra shows consistency with values reported in the literature based solely on GBM data (Nava et al. 2011; Bissaldi et al. 2011), and is able to reproduce a variety of empirical relations presented in the literature, including the $\Gamma^{\rm BAT} - E_{\rm peak}$ and Amati relations. The joint fits do not, in general, give substantially different values for the spectral parameters from the GBM-only analyses.

The updated sample of peak energies shows agreement with the relation between the PL slope of the BAT spectrum and $E_{\rm peak}$ derived previously by Sakamoto et al. (2009) and Zhang et al. (2007b) and indicates the relation's ability to estimate the value of the observed $E_{\rm peak}$ from a fit to the rather narrow *Swift* band. The relation shows a fair amount of scatter, however, and we caution against using it for robust measurements of $E_{\rm peak}$, especially when compared to spectra from *Fermi* or other missions that often contain the spectral peak within the energy range of the detectors. It may be suited, for example, to give a rough estimate of the values of $E_{\rm peak}$ for *Swift* bursts that have no additional observations.

The redshift known subsample of bursts reproduces the general relationship in the $E_{\rm iso} - E_{\rm peak,rest}$ plane and further confirms the conclusions of Gruber et al. (2011) that show generally harder spectra and a larger scatter around the relation than previously believed. Li (2007) proposed the argument that the $E_{\rm iso} - E_{\rm peak,rest}$ relation might evolve with redshift. We believe that the sample of bursts with known redshift, especially the subsample of joint bursts, is still too small to test such a claim. The necessary binning to test the hypothesis would thin out the sample sufficiently to make firm conclusions tenuous at best.

Finally, the interesting discrepancy between the T_{90} derived in the GBM and BAT detectors confirms the soft/hard nature of long/short GRBs, respectively, and suggests the need for a detailed energy-dependent temporal analysis of GRBs.

ACKNOWLEDGMENTS

We would like to thank Taka Sakamoto, Valerie Connaughton, Sylvia Zhu and Binbin Zhang for helpful discussions, David Gruber for providing his $E_{\rm iso}$ and $E_{\rm peak}$ data for comparison with our fits, and the anonymous referee for comments and suggestions that helped improve our manuscript. BZ and FJV acknowledge support from NASA (NNX10AD48G) and NSF (AST-0908362). EWL and YQ acknowledge the support by the National Natural Science Foundation of China (Grants 11025313, 10873002), National Basic Research Program ("973" Program) of China (Grant 2009CB824800), and Guangxi Science Foundation (2010GXNSFC013011, 2011-135).

REFERENCES

Amati L., et al. 2002, A&A, 390, 81
Amati L. 2003, ChJAA Suppl., 3 455
Amati L., Guidorzi C., Frontera F., Della Valle M., Finelli F., Landi R., Montanari E. 2008, MNRAS, 391, 577
Amati L. 2010, arXiv:1002.2232
Band D. L., Preece R. D. 2005, ApJ, 627, 319
Band D. L., et al. 1993, ApJ, 413, 281
Barthelmy S., Sakamoto T., Holland S. 2010, GCN, 10600, 1
Barthelmy S., et al. 2010a, GCN, 10788, 1
Barthelmy S., et al. 2010b, GCN, 10891, 1
Barthelmy S., et al. 2010c, GCN, 11023, 1
Barthelmy S., et al. 2010d, GCN, 11234, 1

Barthelmy S., et al. 2010e, GCN, 11296, 1
Barthelmy S., et al. 2010f, GCN, 11327, 1
Baumgartner W., et al. 2010a, GCN, 11035, 1
Baumgartner W., et al. 2010b, GCN, 11584, 1
Baumgartner W., et al. 2010c, GCN, 11929, 1
Barthelmy S., et al. 2010a, GCN, 11714, 1
Barthelmy S., et al. 2010b, GCN, 11802, 1
Bissaldi E., et al. 2011, ApJ, 733, 97
Cummings J., et al. 2010a, GCN, 10932, 1
Cummings J., et al. 2010b, GCN, 11453, 1
Cummings J., et al. 2010c, GCN, 11475, 1
Cummings J., et al. 2010d, GCN, 11614, 1
Cui X. H., Liang E. W., Lu R. J. 2005, ChJAA, 5, 151
Gehrels N. et al. 2004, ApJ, 611, 1005
Ghirlanda G., Ghisellini, G., Lazzati, D. 2004, ApJ, 616, 331
Ghirlanda G., Nava L., Ghisellini G., Celotti A., Firmani C. 2009, A&A, 496, 585
Ghirlanda G., Nava L., Ghisellini G. 2010, A&A, 511, A43
Gruber D., et al. 2011, A&A, 531, A20
Kocevski D. 2012, ApJ, 747, 146
Kouveliotou, C. et al. 1993, ApJ, 413, 101
Liang E. W., Zhang B. 2005, ApJ, 633, 611
Li L.-X. 2007, MNRAS, 379, 55L
Krimm H., et al. 2010a, GCN, 10322, 1
Krimm H., et al. 2010b, GCN, 11094, 1
Krimm H., et al. 2010c, GCN, 11624, 1
Markwardt C., et al. 2010a, GCN, 10338, 1
Markwardt C., et al. 2010b, GCN, 11111, 1
Markwardt C., et al. 2010c, GCN, 11332, 1
Markwardt C., et al. 2010d, GCN, 11486, 1
Markwardt C., et al. 2010e, GCN, 11946, 1
Nakar E., Piran T. 2005, MNRAS, 360, L73
Nava L., Ghirlanda G., Ghisellini G., Celotti A. 2011, A&A, 530, A21
Palmer D., et al. 2010a, GCN, 10716, 1
Palmer D., et al. 2010b, GCN, 10850, 1
Palmer D., et al. 2010c, GCN, 11664, 1
Palmer D., et al. 2010d, GCN, 11818, 1
Preece R. D., Briggs M. S., Mallozzi R. S., Paciesas W. S., Band D. L. 2000, ApJS, 126, 19
Qin, Y. et al. 2012, arXiv:1205.1188
Richardson G., Koshut T., Paciesas W., Kouveliotou C. 1996, AIPC, 384, 87
Sakamoto T., et al. 2011, PASJ, 63, 215
Sakamoto T., et al. 2010a, GCN, 10379, 1
Sakamoto T., et al. 2010b, GCN, 11511, 1
Sakamoto T., et al. 2009, ApJ, 693, 922
Sakamoto T., et al. 2006, ApJ, 636, L73
Sakamoto T., et al. 2004, ApJ, 602, 875
Scargle J. D., 1998, ApJ, 504, 405
Stamatikos M., et al. 2010a, GCN, 10864, 1
Stamatikos M., et al. 2010b, GCN, 11001, 1
Stamatikos M., et al. 2010c, GCN, 11367, 1
Stamatikos M., et al. 2010d, GCN, 11866, 1
Ukwatta T., et al. 2010a, GCN, 10404, 1
Ukwatta T., et al. 2010b, GCN, 11018, 1
Ukwatta T., et al. 2010c, GCN, 11374, 1
Ukwatta T., et al. 2010d, GCN, 11533, 1
Yonetoku D., et al. 2004, ApJ, 571, 876
Zhang B., et al. 2007a, ApJ, 655, 989
Zhang B., et al. 2007b, ApJ, 655, L25
Zhang B., et al. 2009, ApJ, 703, 1696
Zhang B. B., et al. 2011, ApJ, 730, 141

Table 1. Joint sample bursts whose time-integrated spectra are best fit by a simple powerlaw model. Γ is the slope of the powerlaw and Δt the time interval used for the fit. Spectra were fit using data in the energy range of 15-150 keV(BAT)+8 keV-40 MeV (GBM). Reported errors are to the 90% level.

GRB name	GBM ID	Δt (s)	Γ	χ^2/dof
080905B	080905705	26.624	$1.62^{0.09}_{-0.09}$	526/530
080928A	080928628	18.432	$1.87^{0.07}_{-0.07}$	537/529
090422A	090422150	13.312	$2.12^{0.24}_{-0.21}$	527/532
090518A	090518080	7.168	$1.65^{0.08}_{-0.07}$	402/421
090927A	090927422	9.216	$1.93^{0.2}_{-0.17}$	689/587
100619A	100619015	102.404	$1.83^{0.05}_{-0.05}$	350/413
100727A	100727238	18.432	$1.91^{0.09}_{-0.09}$	545/533

Table 2. Bursts whose time-integrated spectra are best fit by either a cutoff powerlaw or Band function model. Spectra were fit using data in the 15-150 keV (BAT)+8 keV-40 MeV (GBM) energy range. Errors are to the 90% level.

GRB name	GBM ID	Spectral Model^a	Δt^b (s)	α	β	$E_{\rm peak}$ (keV)	χ^2/dof
080714A	080714745	CPL	28.672	$1.22^{0.13}_{-0.15}$	–	155^{54}_{-31}	401/395
080725A	080725435	CPL	36.864	$1.12^{0.07}_{-0.08}$	–	309^{85}_{-57}	456/408
080727C	080727964	CPL	77.825	$1.13^{0.08}_{-0.09}$	–	191^{41}_{-28}	711/526
080804A	080804972	CPL	26.62	$0.56^{0.12}_{-0.13}$	–	200^{30}_{-23}	465/408
080810A	080810549	CPL	69.633	$1.23^{0.06}_{-0.07}$	–	564^{269}_{-140}	581/528
080905A	080905499	CPL	1.152	$0.25^{0.37}_{-0.5}$	–	586^{431}_{-182}	283/267
080916A	080916406	CPL	69.633	$1.24^{0.1}_{-0.11}$	–	134^{31}_{-19}	402/410
081008A	081008832	CPL	60.417	$1.19^{0.1}_{-0.11}$	–	503^{359}_{-167}	591/526
081012 A	081012549	CPL	18.432	$0.05^{0.18}_{-0.38}$	–	256^{71}_{-46}	506/526
081024A	081024245	CPL	0.256	$1.05^{0.24}_{-0.33}$	–	2170^{2074}_{-2074}	104/103
081102A	081102739	CPL	50.177	$0.84^{0.25}_{-0.28}$	–	80^{16}_{-10}	570/529
081109A	081109293	CPL	40.961	$1.44^{0.14}_{-0.15}$	–	133^{68}_{-31}	548/530
081121A	081121858	Band	21.501	$0.53^{0.16}_{-0.18}$	$2.16^{0.19}_{-0.14}$	175^{31}_{-25}	398/391
081126A	081126899	CPL	51.171	$0.96^{0.1}_{-0.12}$	–	249^{73}_{-47}	425/410
081221A	081221681	Band	39.422	$0.86^{-0.06}_{0.06}$	$3.14^{0.6}_{-0.28}$	81^{3}_{-3}	568/410
081222A	081222204	Band	14.336	$0.85^{0.07}_{-0.08}$	$2.39^{0.33}_{-0.22}$	140^{14}_{-13}	460/371
081226A	081226044	CPL	0.384	$0.9^{0.28}_{-0.33}$	–	418^{496}_{-142}	121/120
090102A	090102122	CPL	37.888	$0.98^{0.04}_{-0.04}$	–	443^{46}_{-39}	499/410
090113A	090113778	CPL	12.288	$1.29^{0.19}_{-0.23}$	–	138^{100}_{-39}	346/348
090129A	090129880	CPL	15.36	$1.53^{0.09}_{-0.1}$	–	163^{91}_{-40}	343/376
090423A	090423330	CPL	14.336	$0.87^{0.37}_{-0.73}$	–	52^{8}_{-6}	517/506
090424A	090424592	Band	19.71	$0.95^{0.02}_{-0.02}$	$2.89^{0.26}_{-0.17}$	155^{5}_{-5}	844/525
090509A	090509215	CPL	26.624	$0.9^{0.2}_{-0.23}$	–	221^{112}_{-58}	572/527
090510A	090510016	CPL	0.896	$0.84^{0.05}_{-0.05}$	–	4482^{658}_{-581}	329/304
090519A	090519881	CPL	18.432	$0.51^{0.28}_{-0.34}$	–	296^{171}_{-85}	532/518
090531B	090531775	CPL	3.072	$0.93^{0.15}_{-0.16}$	–	1911^{1067}_{-713}	371/347
090621B	090621922	CPL	0.128	$0.47^{0.3}_{-0.34}$	–	577^{826}_{-230}	57.2/77
090708A	090708152	CPL	14.336	$0.8^{0.44}_{-0.51}$	–	54^{11}_{-8}	460/496
090709B	090709630	CPL	20.48	$0.92^{0.2}_{-0.22}$	–	121^{32}_{-20}	507/530
090712A	090712160	CPL	53.248	$1.06^{0.11}_{-0.12}$	–	588^{566}_{-204}	492/529
090813A	090813174	CPL	9.725	$1.51^{0.13}_{-0.14}$	–	100^{31}_{-18}	344/338
090904B	090904058	CPL	74.663	$1.28^{0.08}_{-0.08}$	–	139^{19}_{-14}	554/529
090912A	090912660	CPL	123.902	$0.8^{0.22}_{-0.24}$	–	72^{9}_{-7}	536/530
090926B	090926914	CPL	64.513	$0.2^{0.14}_{-0.15}$	–	83^{4}_{-4}	520/529
091020A	091020900	CPL	28.672	$1.36^{0.08}_{-0.08}$	–	266^{97}_{-59}	382/412
091026A	091026550	CPL	15.36	$1.31^{0.15}_{0.17}$	–	272^{235}_{-99}	410/378
091102A	091102607	CPL	9.216	$1.03^{0.15}_{-0.17}$	–	439^{364}_{-157}	514/521
091127A	091127976	Band	11.006	$1.21^{0.13}_{-0.15}$	$2.25^{0.04}_{-0.04}$	35^{3}_{-3}	466/366
091208B	091208410	CPL	13.312	$1.36^{0.09}_{-0.09}$	–	118^{22}_{-15}	486/375
091221A	091221870	CPL	35.841	$1.07^{0.07}_{-0.07}$	–	275^{59}_{-41}	721/529
100111A	100111176	CPL	16.374	$1.59^{0.17}_{-0.21}$	–	203^{122}_{-122}	706/649
100117A	100117879	CPL	0.192	$0.14^{0.39}_{-0.52}$	–	380^{194}_{-122}	93.1/86
100206A	100206563	CPL	0.256	$0.64^{0.2}_{-0.21}$	–	763^{865}_{-269}	109/126
100504A	100504806	CPL	28.672	$1.03^{0.22}_{-0.24}$	–	85^{19}_{-11}	582/528
100522A	100522157	CPL	41.985	$1.54^{0.22}_{-0.18}$	–	59^{21}_{-9}	393/412
100615A	100615083	Band	40.574	$0.91^{0.29}_{-0.38}$	$2.07^{0.20}_{-0.09}$	50^{15}_{-10}	437/410
100625A	100625773	CPL	0.32	$0.69^{0.11}_{-0.12}$	–	572^{189}_{-131}	160/143
100704A	100704149	CPL	23.552	$0.91^{0.09}_{-0.09}$	–	187^{33}_{-23}	584/528
100728A	100728095	CPL	191.487	$0.8^{0.03}_{-0.03}$	–	313^{19}_{-17}	538/411
100728B	100728439	CPL	10.237	$0.93^{0.18}_{-0.2}$	–	105^{22}_{-15}	537/501
100802A	100802240	CPL	41.985	$0.57^{0.37}_{-0.41}$	–	83^{22}_{-12}	684/650
100814A	100814160	CPL	158.722	$1.06^{0.11}_{-0.12}$	–	147^{33}_{-21}	566/526
100816A	100816026	CPL	4.542	$0.5^{0.11}_{-0.12}$	–	139^{13}_{-11}	437/364
100906A	100906576	Band	121.347	$1.44^{0.11}_{-0.59}$	$1.99^{0.23}_{-0.2}$	106^{35}_{-64}	589/526
100924A	100924165	CPL	8.061	$1.16^{0.14}_{-0.17}$	–	172^{68}_{-36}	472/437
101008A	101008697	CPL	14.336	$1.24^{0.17}_{-0.22}$	–	701^{597}_{-597}	422/410
101011A	101011707	CPL	27.645	$1.04^{0.2}_{-0.28}$	–	389^{999}_{-190}	520/524

Table 2 (cont'd)

GRB name	GBM ID	Spectral Model[a]	Δt^b (s)	α	β	$E_{\rm peak}$ (keV)	χ^2/dof
101024A	101024486	CPL	13.312	$0.91^{0.41}_{-0.45}$	–	48^{6}_{-5}	543/504
101213A	101213451	CPL	47.105	$1.26^{0.1}_{-0.12}$	–	423^{410}_{-143}	380/411
101219B	101219686	CPL	51.201	$0.08^{0.39}_{-0.45}$	–	72^{11}_{-8}	738/650
110102A	110102788	CPL	148.486	$1.46^{0.06}_{-0.07}$	–	479^{695}_{-196}	403/411
110106B	110106893	CPL	35.84	$1.4^{0.18}_{-0.2}$	–	111^{59}_{-26}	509/528
110119A	110119931	CPL	68.609	$1.15^{0.11}_{-0.12}$	–	224^{110}_{-56}	555/527
110201A	110201399	CPL	12.288	$0.93^{0.12}_{-0.15}$	–	730^{641}_{-311}	612/595
110213A	110213220	CPL	43.009	$1.56^{0.09}_{-0.1}$	–	85^{18}_{-12}	411/410
110318A	110318552	Band	20.48	$0.82^{0.16}_{-0.19}$	$2.3^{0.4}_{-0.18}$	82^{13}_{-11}	446/394
110402A	110402009	CPL	38.526	$1.4^{0.11}_{-0.13}$	–	914^{3248}_{-495}	618/649
110412A	110412315	CPL	20.48	$0.64^{0.24}_{-0.26}$	–	84^{12}_{-9}	532/528

[a]CPL = Cutoff powerlaw or powerlaw + exponential. 100 keV normalization energy.

[b]Duration of time bin for the evaluation of the time-integrated spectra. This is determined by the duration of the signal of the GBM bursts in RMfit

[c]Several bursts in the table (080727C, 081221, 081222, 090424, 091127, 091208B, 100728A) have χ^2 values larger than about 1.3. These bursts are usually long (20 s $> \Delta t >$ 200s) and/or have multi-peak structure, and show significant spectral evolution over the duration of the burst. Doing a simple time-dependent analysis show the fits improve but the spectral evolution likely drives the larger residuals for the full time interval.

Table 3. GBM and BAT T_{90} values in the 8-1000 keV and 15-150 keV energy ranges, respectively. GBM values are derived with the method described in §2.2 and BAT figures are referenced from the literature (see reference column for appropriate citations).

GRB name	GBM ID	GBM T_{90} (s)	BAT T_{90} (s)	Reference[a]
080714	GRB080714745	6.34±0.36	25.81	bat2
080725	GRB080725435	22.21±0.23	92.74	bat2
080727C	GRB080727964	35.55±0.59	77.61	bat2
080804	GRB080804972	73.41±0.93	37.19	bat2
080810	GRB080810549	49.34±0.63	107.67	bat2
080905A	GRB080905499	1.06±0.30	1.02	bat2
080905B	GRB080905705	192.8±1.15	101.62	bat2
080916A	GRB080916406	44.26±0.72	61.35	bat2
080928	GRB080928628	24.54±0.44	233.66	bat2
081008	GRB081008832	175.2±1.16	179.52	bat2
081012	GRB081012549	12.8±0.56	25.2	bat2
081024A	GRB081024245	0.13±0.18	1.82	bat2
081025	GRB081025349	23.62±0.49	22.78	bat2
081101	GRB081101491	0.54±0.39	0.18	bat2
081102	GRB081102739	29.47±0.59	48.19	bat2
081109A	GRB081109293	27.46±0.65	221.49	bat2
081121	GRB081121858	17.98±0.42	17.67	bat2
081126	GRB081126899	35.36±0.46	57.65	bat2
081221	GRB081221681	45.82±0.99	33.91	bat2
081222	GRB081222204	26.75±0.53	33	bat2
081226A	GRB081226044	0.48±0.20	0.44	bat2
090102	GRB090102122	29.02±0.54	29.3	bat2
090113	GRB090113778	8.58±0.29	9.1	bat2
090129	GRB090129880	14.02±0.23	17.66	bat2
090422	GRB090422150	–	8.47	bat2
090423	GRB090423330	12.35±0.50	9.77	bat2
090424	GRB090424592	45.79±0.61	49.47	bat2
090509	GRB090509215	261.18±1.08	336.38	bat2
090510	GRB090510016	0.38±0.045	5.66	bat2
090516A	GRB090516353	85.28±0.54	208	bat2
090518	GRB090518080	7.97±0.44	85.82	bat2
090519	GRB090519881	42.88±0.57	58.26	bat2
090531B	GRB090531775	2.016±0.39	55	bat2
090618	GRB090618353	130.24±1.05	113.34	bat2
090621B	GRB090621922	0.29±0.16	0.14	bat2
090708	GRB090708152	12.48±0.39	8.7	bat2
090709B	GRB090709630	11.14±0.32	27.02	bat2
090712	GRB090712160	31.68±0.62	186.68	bat2
090813	GRB090813174	8.96±0.55	7.14	bat2
090904B	GRB090904058	52.35±0.59	64	bat2
090912	GRB090912660	126.37±0.54	135.52	bat2
090926B	GRB090926914	41.34±0.62	99.28	bat2
090927	GRB090927422	3.2±0.32	2.16	bat2
091020	GRB091020900	44.67±0.65	38.92	bat2
091024	GRB091024372	48.26±0.62	112.28	bat2
091026	GRB091026550	15.74±0.46	174	bat2
091102	GRB091102607	7.58±0.46	6.65	bat2
091112	GRB091112737	50.85±0.82	19.59	bat2
091127	GRB091127976	9.15±0.26	7.42	bat2
091208B	GRB091208410	11.39±0.14	14.8	bat2
091221	GRB091221870	30.432±0.62	68.49	bat2
100111A	GRB100111176	11.01±0.46	12.9	10322
100117A	GRB100117879	0.51±0.19	0.3	10338
100206A	GRB100206563	0.19±0.13	0.12	10379
100212	GRB100212588	8.10±0.46	136	10404
100413A	GRB100413732	78.11±1.07	191	10600
100427A	GRB100427356	10.43±0.41	–	–

Table 3 (cont'd)

GRB name	GBM ID	GBM T_{90} (s)	BAT T_{90} (s)	Reference[a]
100504A	GRB100504806	24.51±0.73	97.3	10716
100522A	GRB100522157	37.38±0.59	35.3	10788
100615A	GRB100615083	36.42±0.59	39	10850
100619A	GRB100619015	92.61±0.34	97.5	10864
100625A	GRB100625773	0.38±0.14	0.33	10891
100704A	GRB100704149	11.81±0.54	197.5	10932
100727A	GRB100727238	25.92±0.47	84	11001
100728A	GRB100728095	159.97±0.76	198.5	11018
100728B	GRB100728439	9.34±0.46	12.1	11023
100802A	GRB100802240	132.26±0.84	487	11035
100814A	GRB100814160	25.41±0.29	174.5	11094
100816A	GRB100816026	2.24±0.23	2.9	11111
100906A	GRB100906576	115.56±0.68	114.4	11234
100924A	GRB100924165	11.87±0.43	96	11296
101008A	GRB101008697	7.2±0.30	104	11327
101011A	GRB101011707	38.50±0.62	71.5	11332
101023A	GRB101023951	66.94±0.55	80.8	11367
101024A	GRB101024486	20.51±0.54	18.7	11374
101129A	GRB101129652	0.544±0.17	–	–
101201A	GRB101201418	83.62±0.68	–	–
101213A	GRB101213451	38.24±0.56	135	11453
101219B	GRB101219686	54.21±0.75	34	11475
101224A	GRB101224227	0.56±0.32	0.2	11486
110102A	GRB110102788	133.76±0.34	264	11511
110106B	GRB110106893	22.78±0.62	24.8	11533
110119A	GRB110119931	59.87±0.59	208	11584
110128A	GRB110128073	–	30.7	11614
110201A	GRB110201399	11.712±0.51	13	11624
110207A	GRB110207470	39.01±0.52	80.3	11664
110213A	GRB110213220	33.12±0.46	48	11714
110318A	GRB110318552	14.66±0.41	16	11802
110319B	GRB110319815	13.95±0.52	14.5	11818
110402A	GRB110402009	35.19±0.53	60.9	11866
110412A	GRB110412315	17.4±0.53	23.4	11929
110420B	GRB110420946	0.74±0.25	0.084	11946

[a]References for BAT T_{90}: bat2 - Second BAT Catalog (Sakamoto et al. 2011). Other numbers in this column correspond to GCN reports. See bibliography for full record information.

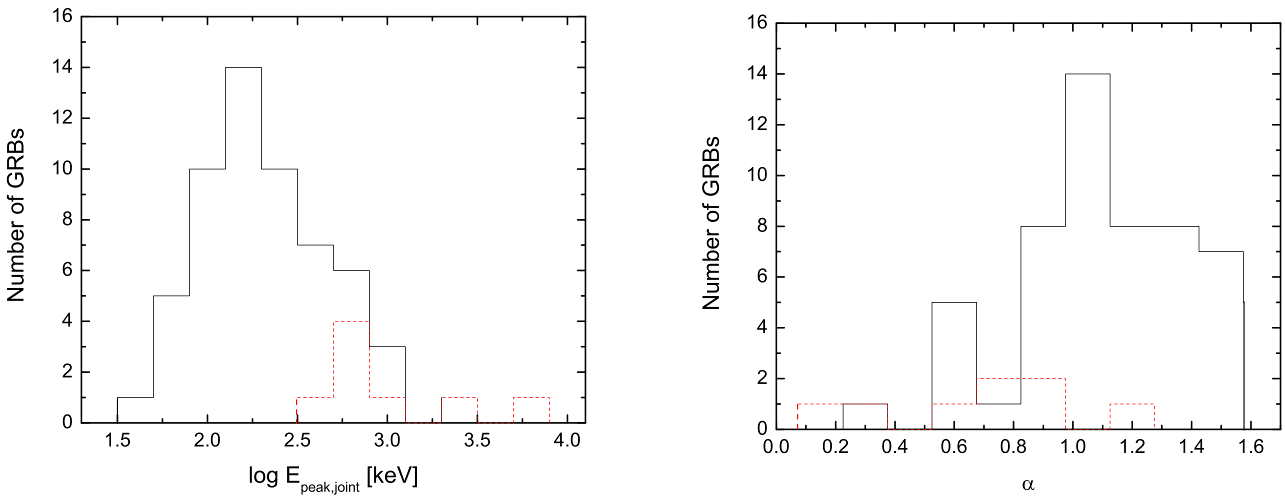

Figure 1. Distributions of $E_{\rm peak}$ and α for the best fit joint sample bursts. Both are generally consistent with the literature (e.g. Preece et al. 2000; Zhang et al. 2011; Nava et al. 2011). The solid (black) and dashed (red) histograms are for long and short GRBs, respectively.

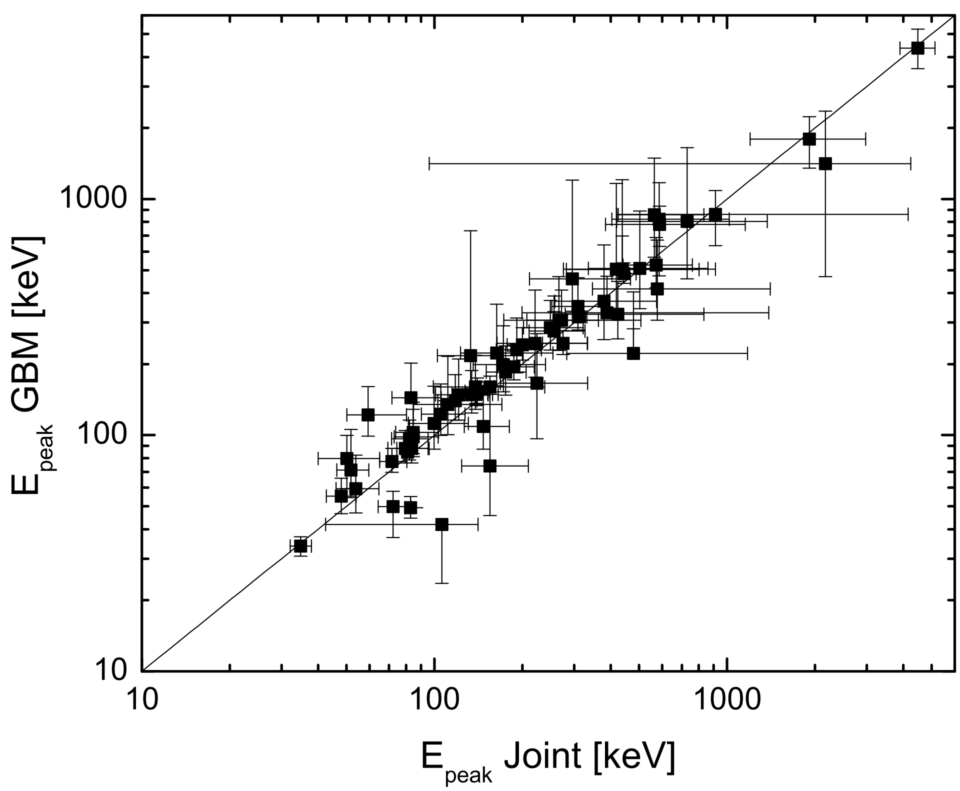

Figure 2. The relationship between the best fit $E_{\rm peak}$ for the joint sample and the GBM spectra. The line superimposed is the line with slope 1. This shows that adding the BAT data into the fit does not significantly change the values of $E_{\rm peak}$.

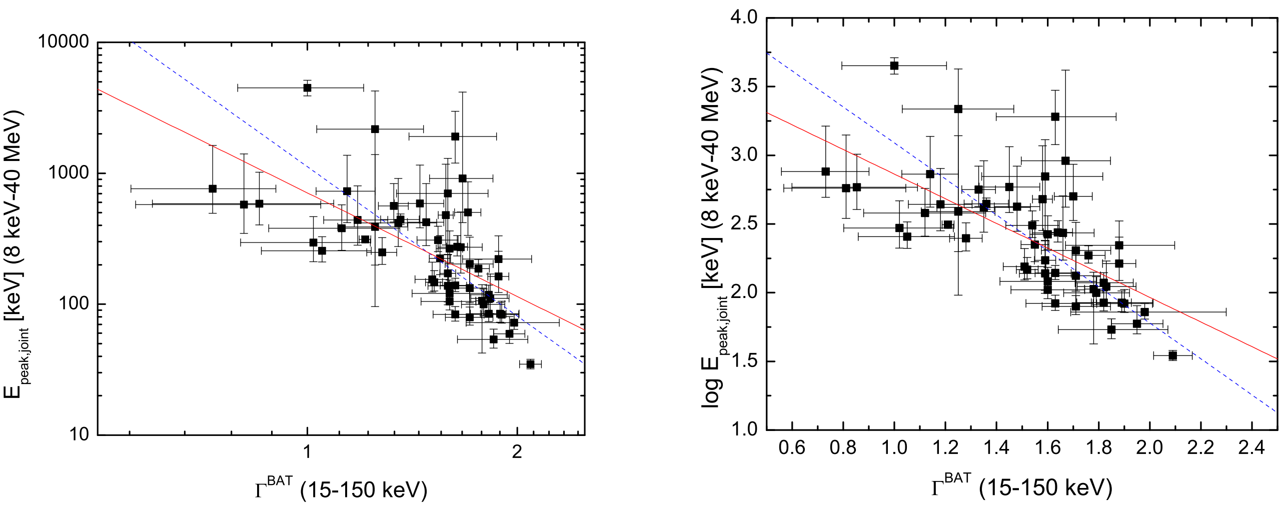

Figure 3. The $\Gamma^{\rm BAT} - E_{\rm peak}$ relation in both log-log (a) and log-linear (b) space created from 53 best-fit spectra. 15 bursts were removed from the original sample of 75 because the BAT best-fit model was a CPL and not a simple PL. An additional seven bursts were removed because the joint spectrum is described by a simple PL. As shown below, the difference in $E_{\rm peak}$ between the CPL and Band model fit for the joint spectra is negligible, so the best-fit model value was used. The lines superimposed on the plots are the best-fit lines generated using an ordinary least squares fit (red, solid) and a least squared linear bisector fit (blue, dash) that considers some of the scatter in the relation. The latter procedure's parameters are summarized in the text.

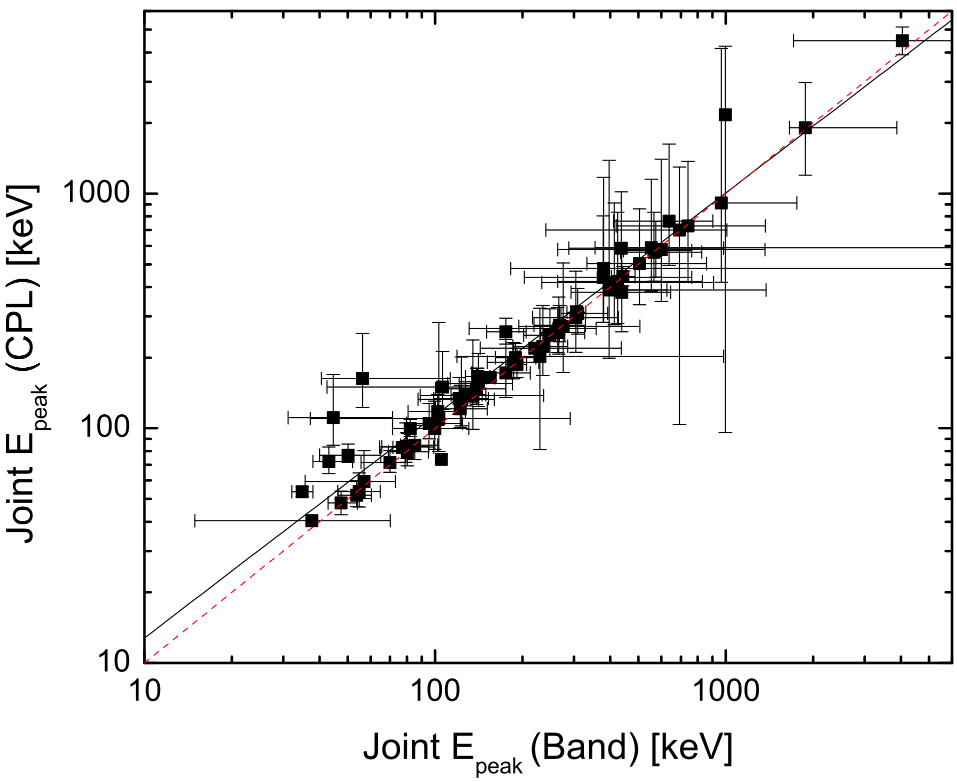

Figure 4. The relationship between the values joint $E_{\rm peak}$ for a CPL and Band model for all 75 GRBs in our sample. The best fit line (solid, black) has a slope of nearly 1, as shown by the reference line (dashed, red), with very few outliers from this relation. Such small changes in the value are negligible in the global analysis of spectral properties and we, therefore, always take the best-fit model value of $E_{\rm peak}$. Some Band function fits are not well constrained and are reflected in the large horizontal error bars for some bursts.

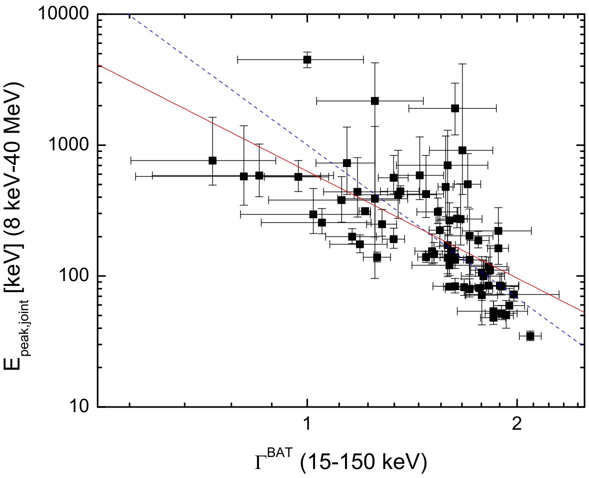

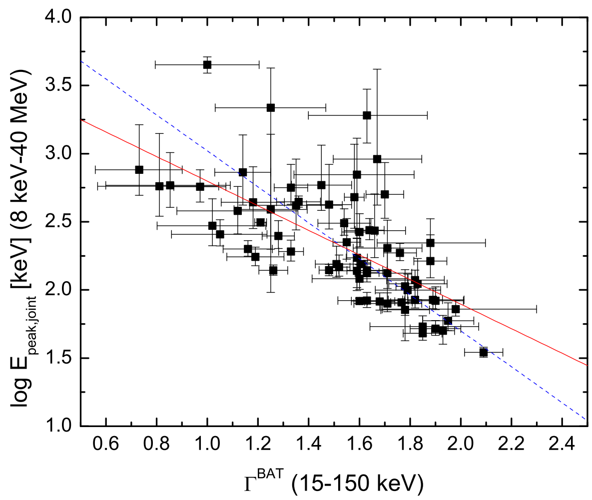

Figure 5. The $\Gamma^{\rm BAT} - E_{\rm peak}$ relation in both log-log (a) and log-linear (b) space created from all the bursts in our sample. We refit the *Swift* bursts that are described as a CPL with a simple PL model and use this value of Γ, regardless of the increase in the χ^2. The lines superimposed on the plots are the best-fit lines generated using an ordinary least squares fit (red, solid) and a least squared linear bisector fit (blue, dash) that considers some of the scatter in the relation. The latter procedure's parameters are summarized in the text.

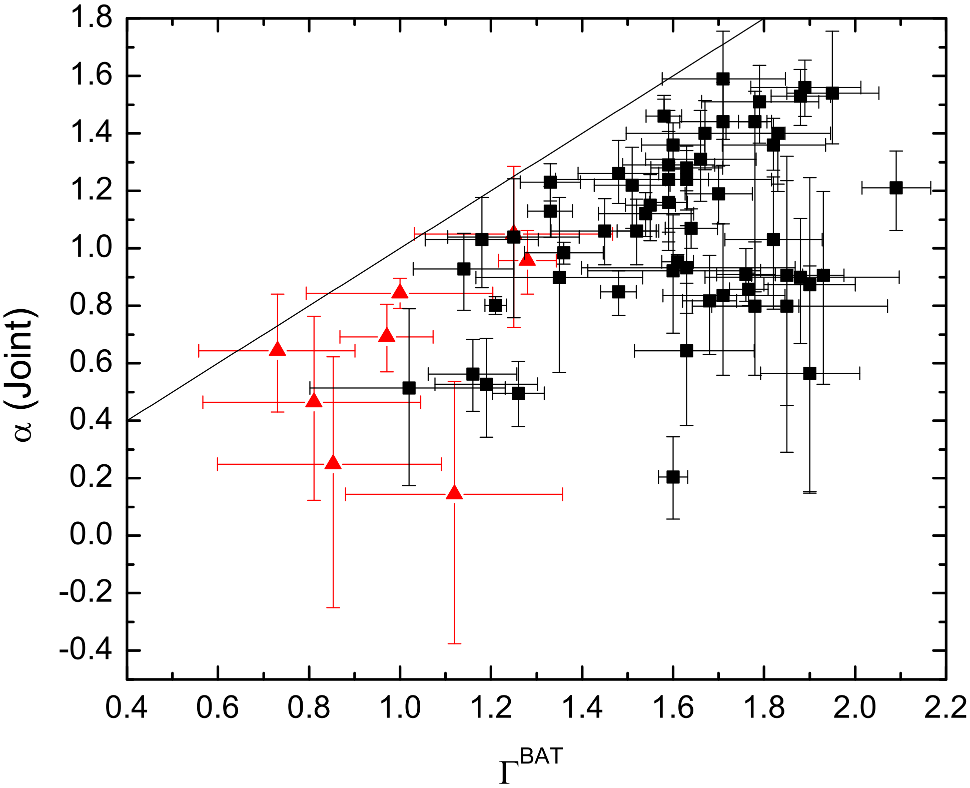

Figure 6. Relationship between the BAT PL spectral slope $\Gamma^{\rm BAT}$ and the joint fit CPL/Band α for short (red, triangle) and long (black, square) bursts. The line superimposed is a reference of slope = 1.

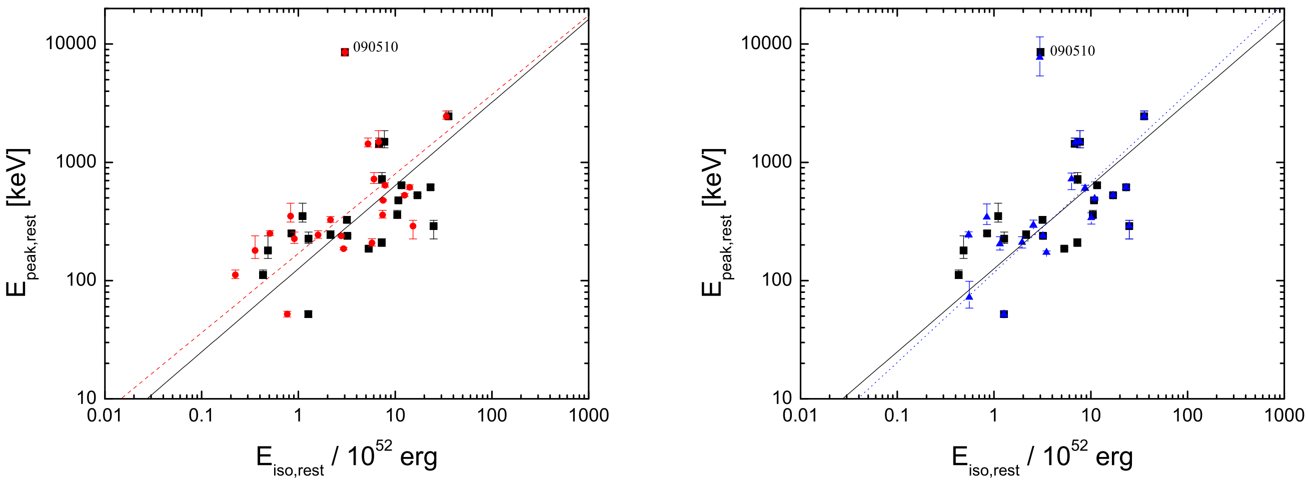

Figure 7. Alternative methods for calculating the relationship between $E_{iso,rest}$-$E_{peak,rest}$. In both panels, the black (square) icons and the solid black line are identical to those presented in Figure 8. The dashed line represents the best linear bisector fit to the second data set for reference. Short burst 090510 is labelled but not included in the calculations. (a) Rest frame fluxes are calculated assuming a CPL spectrum (red/circle) instead of a Band function (black/square, identical to Fig 8). This systematically underestimates the isotropic energy by a mean factor of about 1.4. (b) Rest frame fluxes calculated using Band function parameters, even if a CPL gives a better fit (i.e. lower χ^2; blue/triangle). If β cannot be constrained a typical value of -2.3 is assumed. This gives a similar distribution to that produced in Figure 8 (black/square).

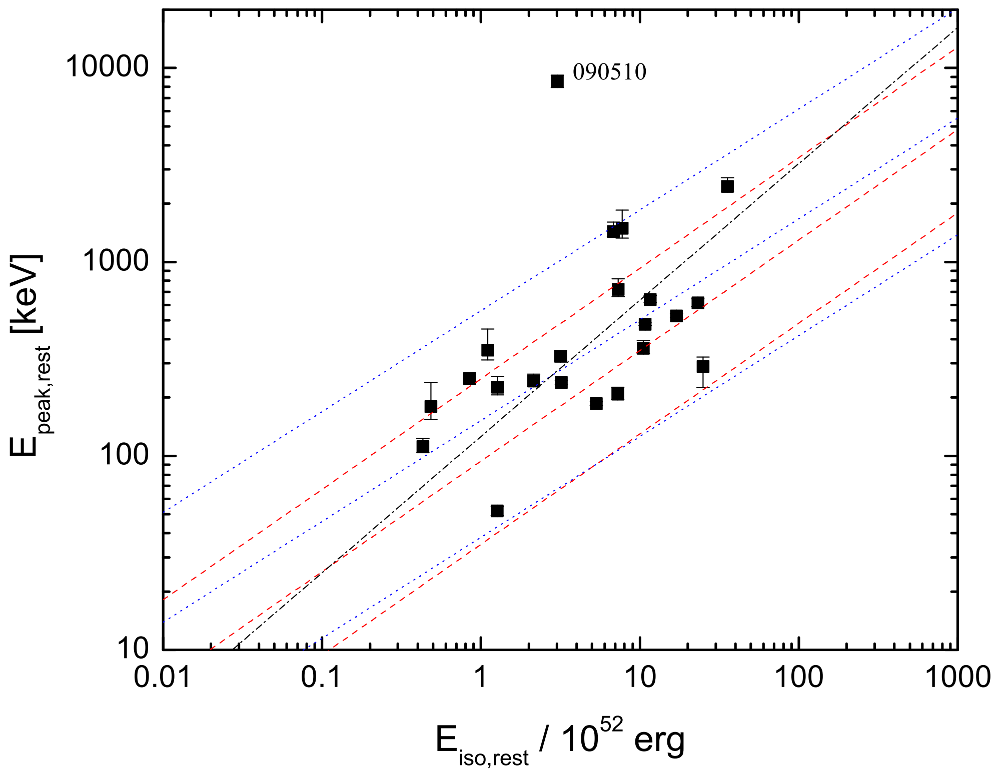

Figure 8. Relationship between the isotropic equivalent energy release and the peak energy of the time-integrated spectrum of the joint sample bursts. Isotropic energies are derived using a Band function spectrum. If the spectrum is best described by a CPL then the best-fit pre-break slope (α) is used with the assumption of a typical β of -2.3 to construct a Band function. Superimposed are the best ordinary least squares bisector fit of the joint sample (black/dash-dot, slope=0.76) and the approximate best fit lines and 2σ regions reported in Amati et al. (2008; red/dashed; slope=0.57) and Gruber et al. (2011; blue/solid; slope=0.52). The shift to steeper slopes is produced from a lack of bursts above $E_{\rm iso} \sim 10^{54}$ erg, which is attributed to a selection effect of the sample. These bursts are the highest energy bursts detected and are *Fermi* LAT triggers and therefore do not show up in our sample of joint GBM-BAT bursts. If these highest energy bursts are introduced to create a more complete sample, we show consistency with both slope values presented in the literature. We also confirm the larger scatter and slightly harder spectra presented by Gruber et al. (2011). Differences in the absolute values of $E_{\rm peak}$ are likely due to the derivation of the parameter using the joint BAT-GBM data. The obvious outlier in the distribution is GRB 090510 (labelled), the only short burst ($T_{90} < 2$ sec) in the redshift-known subsample. This burst is not used in calculating the best-fit line. Previous works (Amati et al. 2008; Zhang et al. 2009; Ghirlanda et al. 2009; Amati et al. 2008) have shown that these bursts follow a different relationship in the $E_{\rm peak,rest} - E_{\rm iso}$ plane and are not considered in the fitting of the slope of the relation.

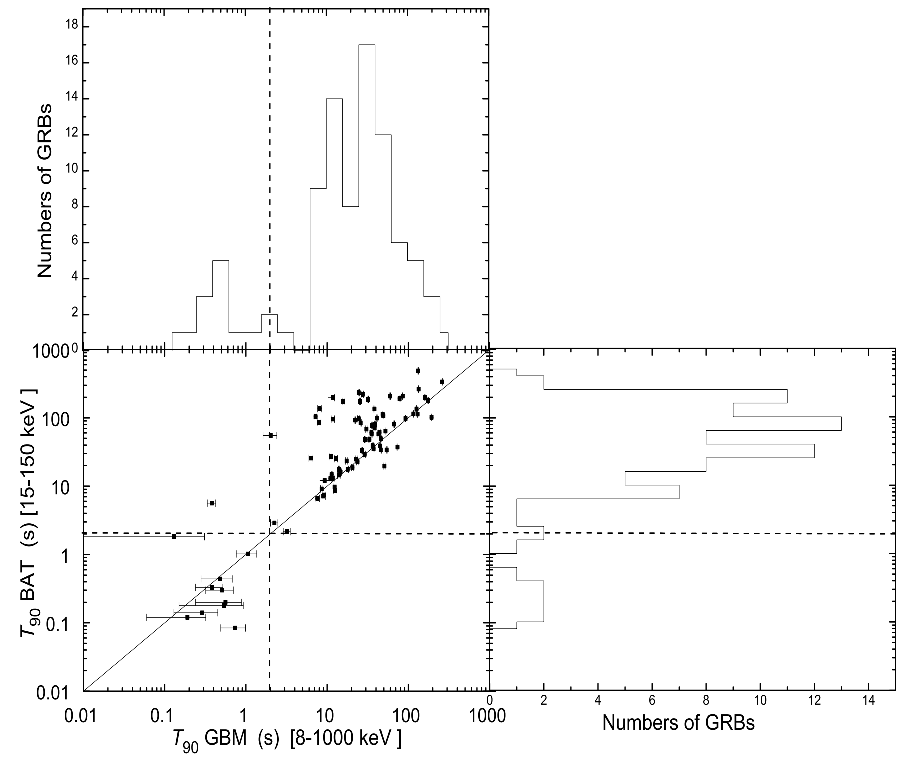

Figure 9. T_{90} measures for the joint sample bursts as derived with the BAT (15-150 keV) and GBM (8-1000 keV)data and corresponding distributions. The diagonal solid line is the line of slope = 1, while the dashed lines indicate a duration of 2 sec. Note the typically longer durations in the *Swift* band for the long and generally softer bursts while the trend reverses for the shorter, typically softer, bursts.